Bayesian analysis of the effective charge from spectroscopic bremsstrahlung measurement in fusion plasmas

M. Krychowiak, R. König, and T. Klinger
Max-Planck-Institut für Plasmaphysik, EURATOM Association, Wendelsteinstrasse 1, Greifswald 17491, Germany

R. Fischer
Centre for Interdisciplinary Plasma Science, Boltzmannstrasse 2, Garching 85748, Germany

(Received 22 April 2004; accepted 6 July 2004)

At the stellarator Wendelstein 7-AS (W7-AS) a spectrally resolving two channel system for the measurement of line-of-sight averaged Z_{eff} values has been tested in preparation for its planned installation as a multichannel Z_{eff}-profile measurement system on the stellarator Wendelstein 7-X (W7-X) which is presently under construction. The measurement is performed using the bremsstrahlung intensity in the wavelength region of ultraviolet to near infrared. The spectrally resolved measurement allows to eliminate signal contamination by line radiation. For statistical data analysis a procedure based on Bayesian probability theory has been developed. With this method it is possible to estimate the bremsstrahlung background in the measured signal and its error without the necessity to fit the spectral lines. For evaluation of the random error in Z_{eff} the signal noise has been investigated. Furthermore, the linearity and behavior of the charge-coupled device detector at saturation has been analyzed. © *2004 American Institute of Physics*. [DOI: 10.1063/1.1787135]

I. INTRODUCTION

The effective ionic charge Z_{eff} of fusion plasmas is often determined from the bremsstrahlung emission in visible or near infrared spectral band. One well-established method is based on spectral integration of plasma light using interference filters. The technique is useful for high plasma temperatures where recombination radiation is usually negligible. However, due to decrease of the plasma temperature towards the plasma edge, the bremsstrahlung spectrum is superimposed by an increasing number of emission lines. Since the interference filter technique does not allow one to separate between bremsstrahlung and line emission, this method is always prone to misinterpretations.

This problem can be avoided by using narrow spectral windows ($\Delta\lambda \approx 1$ nm), which are known to be usually free of line radiation (e.g., at $\lambda = 523.5$ nm[1]). Another possibility is to perform such spectrally integrating measurements with more than one spectral window (usually 3–4) for each line of sight [at stellarator Wendelstein 7-AS (W7-AS) the observation system of the Thomson scattering diagnostic can be used[2]]. This allows the reconstruction of the radial Z_{eff} profile using signals from those spectral windows which are believed to contain the least line radiation contribution. A further reduction of the influence of line radiation can only be obtained by deriving Z_{eff} from spectrally resolved measurements, which allow the determination of the continuous bremsstrahlung background in the presence of line radiation. This was done by fitting the appearing spectral lines in the measured spectra of the visible charge exchange spectroscopy diagnostic at the Joint European Torus.[3]

In the present paper a robust method is used for estimating Z_{eff} from the bremsstrahlung measurement in the presence of additional line emission without fitting spectral lines. The method is robust with respect to line radiation contributions, because the spectral resolution of the system of about 1 nm is sufficient for the identification of several spectral regions that are not contaminated by line radiation. For this purpose a broad spectral range of $\Delta\lambda \approx 500$ nm is covered by the spectrometer. The contaminated spectral regions are dealt with as outlier data by employing a Bayesian mixture modeling technique. This technique is based on a probabilistic approach which allows for a robust fit of a model function to a set of noisy data in the presence of outliers without preprocessing of the data.[4] The data do not have to be censored because both regular and outlier data can be used for the fitting procedure.

Section II summarizes the physical model of the bremsstrahlung intensity, Sec. III describes the experimental setup, Sec. IV shows the noise calibration of the experimental data, Sec. V depicts the saturation behavior of the detector, Sec. VI describes the Bayesian approach to separate the bremsstrahlung background from the line emission, Sec. VII shows results, and Sec. VIII summarizes.

II. BREMSSTRAHLUNG MODEL

Z_{eff} is obtained from the bremsstrahlung intensity. Its emission coefficient is given by[5]

$$\varepsilon_{\lambda}^{ff} = \overline{g}^{ff} \frac{8\pi e^6 \sqrt{2}}{3(4\pi\varepsilon_0)^3 m_e^{3/2} c^2 \sqrt{3\pi}} \frac{n_e^2 Z_{\mathrm{eff}}}{\lambda^2 \sqrt{k_B T_e}} \exp\left(-\frac{hc}{\lambda k_B T_e}\right), \tag{1}$$

where λ is the wavelength, T_e the electron temperature, and n_e the electron density. The temperature-averaged free-free Gaunt factor $\overline{g}^{ff}$ includes the quantum mechanical correction and can be approximated for our temperature and wavelength range by[6]

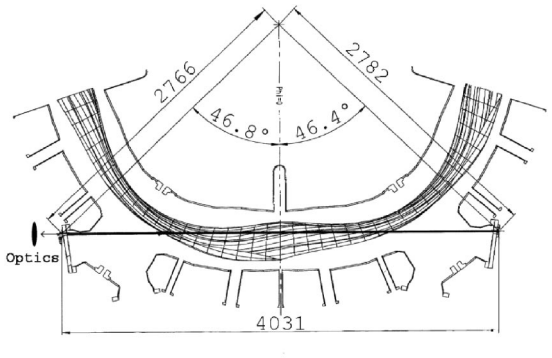

FIG. 1. Line of sight of the spectrometer on the horizontal plane ($z=0$) with the coordinates R (large plasma radius in mm) and ϕ (toroidal angle).

$$\overline{g}^{ff} = 1.35 T_e^{0.15}[\mathrm{eV}]. \tag{2}$$

Inserting the numerical values for the constants we obtain the following expression for Z_{eff}:

$$Z_{\mathrm{eff}} = \varepsilon_\lambda^{ff} \frac{\lambda^2 T_e^{0.35}}{2.045 \times 10^{-29} n_e^2 \exp(-12\,400/\lambda T_e)}, \tag{3}$$

where ε_λ^{ff}, λ, T_e, and n_e are expressed in units of W cm^{-3} Å^{-1} sr^{-1}, Å, eV, and cm^{-3}, respectively.

III. EXPERIMENTAL SETUP

W7-AS is a "partially optimized," low shear modular stellarator with nonplanar Cu coils. It has five magnetic field periods. The major and minor radii are $R=2$ m and $a \leqslant 0.16$ m, respectively. The magnetic field strength at the axis is $B \leqslant 2.5$ T. The rotational transform ι can be varied between 0.25 and 0.6 by currents in a set of planar coils.

The plasma radiation is integrated along two horizontal ($z=0$) toroidal lines of sight (Fig. 1). Since they are nearly identical (the end points of both lines differ by about 3 cm), one obtains as result two line-of-sight averaged Z_{eff} values which coincide within the error bars. The weighting factors for the Z_{eff} averaging along the lines of sight are mainly given by the squared electron densities at the emission points.

Z_{eff} is measured with a small Ocean Optics two-channel spectrometer S2000 covering the spectral regions of 247–573 nm [ultraviolet-visible (UV-VIS) channel] and 475–1121 nm [visible-near infrared (VIS-NIR) channel]. The plasma light is reflected on a mirror and focused by a lens (UV-VIS-IR achromat, diameter 13 mm, focal length 50 mm).

A coupler with two glass fibers of diameter 600 μm is mounted to the lens such that the ends of both fibers are located in the focus of the lens. Both fibers of length 50 m (one of them made from quartz glass because of its higher transmission in the UV region) are connected to the spectrometer in the W7-AS control room.

The 50 μm wide slit and fixed gratings of 1200 lines/mm (UV-VIS channel) and 600 lines/mm (VIS-NIR channel) yield spectral resolutions of 1 nm (UV-VIS channel) and 2.2 nm (VIS-NIR channel), respectively. Cylindrical lenses are located on the detectors of both channels imaging the 600 μm slit height onto the 200 μm detector height.

A long pass filter, which transmission edge is increasing with the pixel number (wavelength), is coated onto the detector of the UV-VIS channel. This eliminates the second-order effects in all pixels. The VIS-NIR channel is equipped with a simple long pass filter with constant transmission edge for all pixels at $\lambda=475$ nm, making the wavelength region of $\lambda>920$ nm unusable because of second-order effects.

Both channels are equipped with a 2048 element linear silicon charge-coupled device (CCD) array of 14×200 μm elements (the first 24 are covered for dark current measurement). The pixel charges are converted into 12-bit values by an 1 MHz analog-to-digital (A/D) converter (PCI card). The minimal exposure time is 7 ms per channel.

The spectrometer is wavelength-calibrated using Hg, Cd, and Ne spectral lamps. For the absolute calibration, an Ulbricht sphere of 50 cm diameter has been used. Recording of the Ulbricht sphere light was done with the same optical components as during experiments, except for the window glass which could not be removed from the torus at the time of the calibration. The window transmission has been measured afterwards. The absolute calibration with the Ulbricht sphere is possible only for wavelengths $\lambda>300$ nm. Moreover, in the range of $300<\lambda<400$ nm the calibration is not reliable because of low radiation. Consequently, the spectral region of $\lambda<400$ nm was excluded from the analysis of the UV-VIS channel experimental data and the spectral region to be analyzed is $\lambda=400-920$ nm.

Figure 2(a) shows an example of plasma light measurement with both spectrometer channels. The two spectra overlap in the region $\lambda=475-573$ nm. The $1/\lambda^2$ dependence of the background radiation is recognized in the region without second-order radiation ($\lambda<920$ nm). Figure 2(b) depicts the Z_{eff} values as calculated from Eq. (3) using the measured radiation data plotted in Fig. 2(a). Z_{eff} does not depend on λ. Thus, the flat baseline shows that recombination radiation plays no role and Z_{eff} can be estimated from the bremsstrahlung intensity. The intensity excursions in the Z_{eff} spectrum are due to line radiation.

IV. SIGNAL NOISE AND DETECTOR LINEARITY

For the correct estimation of Z_{eff} the uncertainty of the measured data has to be determined and the detector linearity must be proven.

The uncertainty of a CCD detector signal originates from photon and electron-hole pair counting statistics and detector noise. The counting statistics results in a Poisson distribution of electron-hole pairs which is approximated by a Gaussian distribution with variance σ^2. The detector variance σ_D^2 consisting of readout noise and electronic offset noise is assumed to be constant. To the signal L an offset O is added electronically, $D=L+O$, to prevent the A/D converter from underflow. Since one is interested in the signal L resulting from the incoming photon intensity, the subtraction of the offset O from the total signal D enhances the uncertainty by $2\sigma_D^2$ (Ref. 7) and one obtains

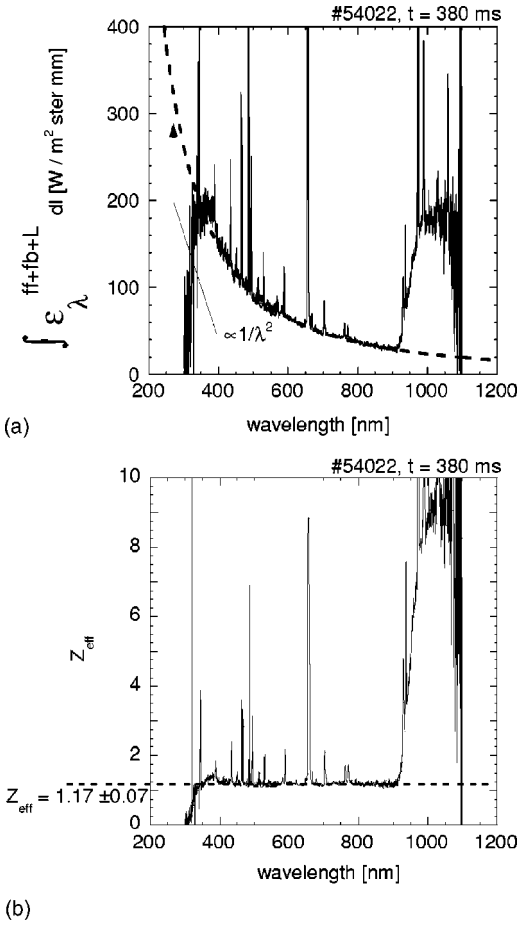

FIG. 2. (a) Spectrum of the line-integrated total radiation coefficient measured by two spectrometer channels at W7-AS. (b) Line-averaged Z_{eff} derived from the total radiation coefficient from (a). The $1/\lambda^2$ dependence of the intensity background curve [dashed line in (a)] and constancy of this curve in (b) are clear evidence that recombination radiation can be neglected.

$$\sigma_L^2 = \frac{1}{u}L + 2\sigma_D^2, \tag{4}$$

where u is a conversion factor between electron-hole-pair counts and analog-to-digital units (ADUs).

Figure 3 shows the result of the noise calibration measurement. Hundred identical measurements on the VIS-NIR channel have been made with the Ulbricht sphere. Figure 3 shows the variance σ_L^2 of the different pixels, plotted against the mean signal $\langle L \rangle$. The exposure time of 33 ms was chosen such that the full A/D range (4096 ADU) was used. Assuming photon or electron-hole pair creation statistics we expect to have a linear relation between the measured intensity and the variance. The measured curve is linear for $L < 1000$ ADU but deviates from linearity for intensities $L > 1000$ ADU.

The reason for the nonlinearity behavior is unknown. It seems that the conversion factor u depends on intensity L. We can exclude that the detector response is nonlinear with respect to L because the measured intensity for single pixels depends linearly on the exposure time between 8 and 33 ms. In addition, we can exclude that u depends on the pixel index

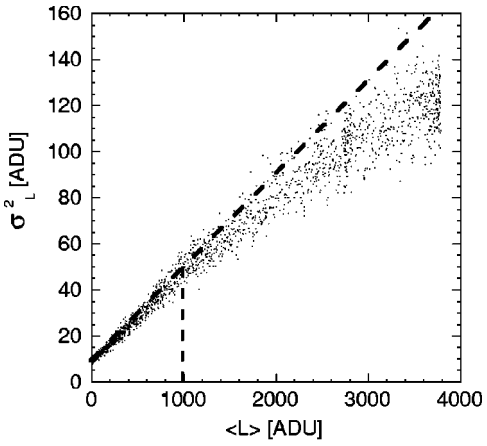

FIG. 3. Measurement of the signal variance from 100 exposures to the Ulbricht sphere light (33 ms long) plotted versus the average intensity.

because measurements on single pixels with different mean intensities (exposure time 8–33 ms) show the same nonlinear dependence as in Fig. 3.

Even though the measured variance behavior plotted in Fig. 3 has not been completely understood, it can be used for error analysis of the Z_{eff} estimation. The variance is approximated by a second-order polynomial

$$\sigma_L^2 = \frac{1}{23.1}L + 8.3 - 3.4 \times 10^{-6}L^2. \tag{5}$$

The UV-VIS channel shows a similar behavior

$$\sigma_L^2 = \frac{1}{24.3}L + 6.1 - 4 \times 10^{-6}L^2. \tag{6}$$

V. SATURATION BEHAVIOR OF THE DETECTOR

In most cases measured signals of the bremsstrahlung intensity from the plasma are below the detector saturation limit. Nevertheless, the experimental spectra may exhibit pronounced spectral lines (mostly H_α), which may locally saturate the detector. For this reason it is important to know to what extent a saturated line disturbs the signals of the remaining nonsaturated pixels.

The detector is composed of a light-sensitive linear CCD array and a readout shift register (consisting of 2048 pixels as well). After each light exposure, the charges collected in the CCD pixels are directed in parallel to the readout register. After that, the CCD array is ready for the next light exposure. The charges in the pixels of the readout register are shifted pixel by pixel for conversion into digital values by an A/D converter. The readout time of all pixels is determined by the clock rate of the A/D converter of 1 MHz and accounts for $\approx$2 ms. Directly before the next charge transport from the CCD array to the readout register, it undergoes a clear cycle, i.e., the pixels of the readout register are once again shifted towards its first pixel in order to remove all charges.

If a saturated CCD pixel is further illuminated, the generated charge excess could leak either into adjacent pixels of the CCD array or into pixels of the readout register. In the

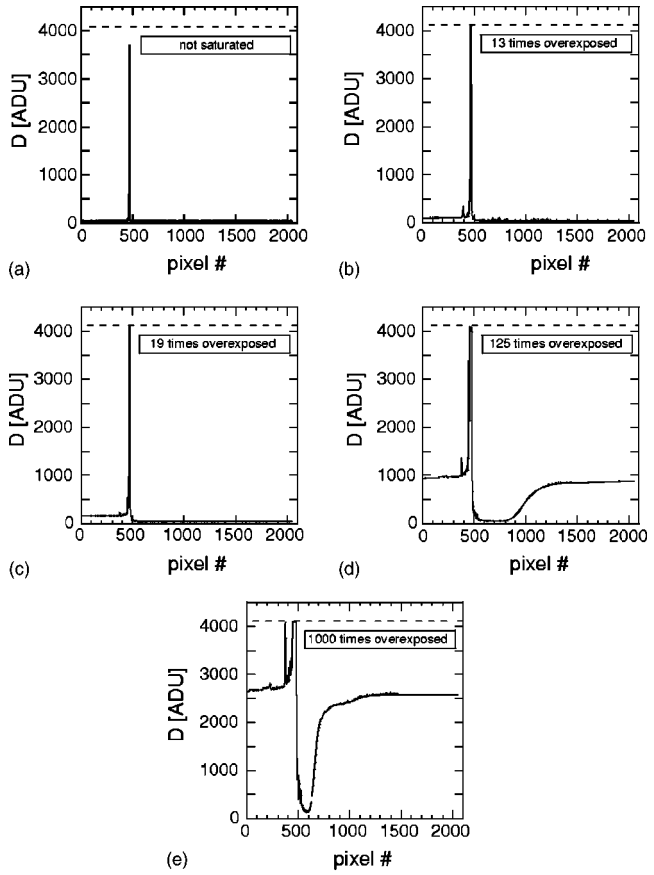

FIG. 4. He-Ne laser light exposed for 6 ms duration to the VIS-NIR channel. By using different gray filters, different levels of detector overexposure were studied.

first case one would observe simply an increase of the adjacent pixels signals. In the second case one could expect two effects which are as follows.

(1). During the clear cycle the pixels of the readout register that pass the saturated (and illuminated) CCD pixels can receive leak charge.

(2). If, during the readout time of 2 ms, a CCD pixel becomes saturated, its charges can also leak to the passing pixels of the readout register.

In order to check the importance of these effects for our detectors, the VIS-NIR channel has been exposed to the light of an He-Ne laser ($\lambda = 632.8$ nm). The laser light was integrated for 6 ms. Laser attenuation by using different gray filters of known transmission allowed exposures in which the CCD pixels corresponding to $\lambda = 632.8$ nm were either close to saturation [Fig. 4(a)] or overexposed by factors of 13, 19, 125, and 1000 [s. 4(b)–4(e), respectively].

The measured data can be explained as follows: All pixels on the left-hand side (lhs) of a saturated line (including the first 24 pixels used to determine the offset) receive leak charge during the clear cycle (which one can imagine on . 4 as a shift to the left). The leak signal increases with light intensity. This can be seen in all cases with saturation [s. 4(b)–4(e)]. The signal increase on the right-hand side (rhs) of the line, which also increases with light intensity, is caused by the readout procedure: If during the readout time of about 2 ms any CCD pixel becomes saturated and is further illuminated, the charges begin to leak into the passing pixels of the readout register. Although towards the end of the readout procedure the pixels on the lhs of the line (which already have been read out) receive leak charges as well, this has no effect because of the upcoming clear cycle. So the signal enhancement, caused by the readout procedure, affects the pixels on the rhs of the line only.

A more detailed analysis of the leak signals shown in Figs. 4(d) and 4(e) leads to following two conclusions.

(1). Leakage on the rhs of a saturated line (generated during the readout procedure) sets in after the line has been overexposed by about a factor of 6.

(2). The next exposure starts about 0.1 ms after the beginning of the readout procedure.

The first conclusion explains why no leakage on the rhs of the line can be seen in the plots with overexposure by factors of 13 and 19: At the moment when the charge of the 2048th pixel of the readout register passed the overexposed CCD pixel, it was first overexposed by a factor of $(0.1\ \text{ms} + 0.75 \times 2\ \text{ms}) \times 13/6\ \text{ms} = 3.5$ and $(0.1\ \text{ms} + 0.75 \times 2\ \text{ms}) \times 19/6\ \text{ms} = 5$, respectively: less than a factor of 6. In contrast the leak signal on the lhs of the line can be observed in all four cases with saturation [Figs. 4(b)–4(e)] because at the time point of the clear cycle, which is the reason for this leak, the line has already been overexposed by a factor of nearly 13, 19, 125, and 1000, respectively. Therefore this leakage produces a higher signal increase than the leakage on the rhs of the line. Additional measurements have shown that horizontal leaks from overexposed CCD pixels into adjacent CCD pixels only play a role at exposure times of some 100 ms and more. However, such long exposure times have not been used in our experiments.

Keeping in mind the short exposure time (mostly 7 ms) during experiments, the following conclusions can finally be drawn for the evaluation of spectroscopic data from exposures of stationary radiation conditions.

(1). Leakage on the lhs of a saturated line sets in already at a lower overexposure level than leakage on the rhs. If a saturated spectral line appears, no signal spuriousness is expected if the offset (derived from the 24 covered pixels) is nearly the same as in a case without any saturation.

(2). If increased offset is observed, the whole region on the lhs of the line is also spuriously increased by the same value. The region on the rhs of the line may be affected by a smaller amount as well. Nevertheless, there will still be a leak-free region on the left, directly behind the line, which is at least $0.1\ \text{ms}/2\ \text{ms} \times 2048 \approx 100$ pixels wide.

(3). If more than one saturated line appears and the offset is thereby increased, leakages caused by different lines may overlap and seriously disturb the whole spectrum.

(4). Horizontal leakage within the CCD array does not play any role.

Due to these inferences one can, e.g., expect the measured data plotted in Fig. 5(a) to be suitable for the Z_{eff} derivation from the bremsstrahlung, since the offset value is obviously not disturbed despite saturated H_α line. This is further supported by the $1/\lambda^2$ dependence of the background line in Fig. 5(b).

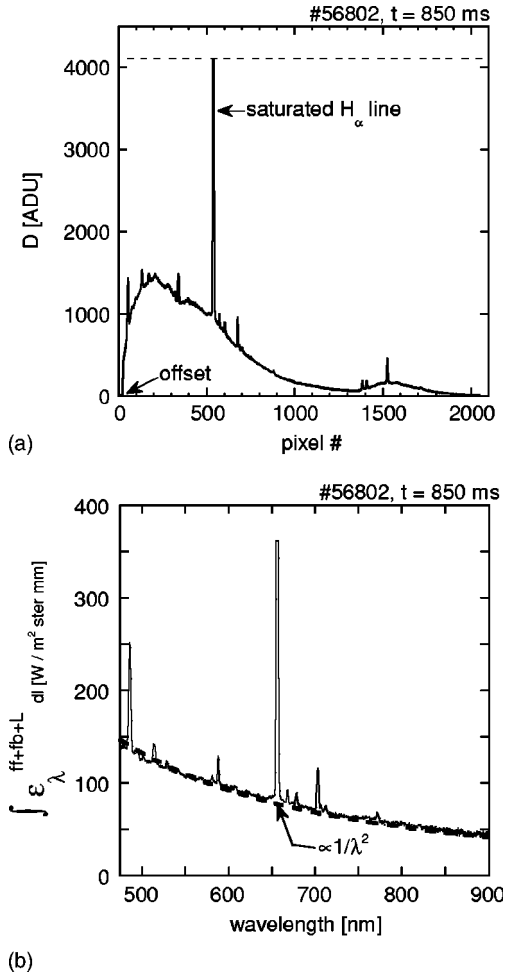

FIG. 5. (a) Measurement of plasma radiation in discharge No. 56802, $t = 850$ ms with one saturated line. Despite the saturation of the H_α line the fact that the offset value is not affected indicates that the whole spectrum does not get disturbed. (b) The $1/\lambda^2$ dependence of the background line of the line-integrated radiation coefficient confirms the prediction from (a).

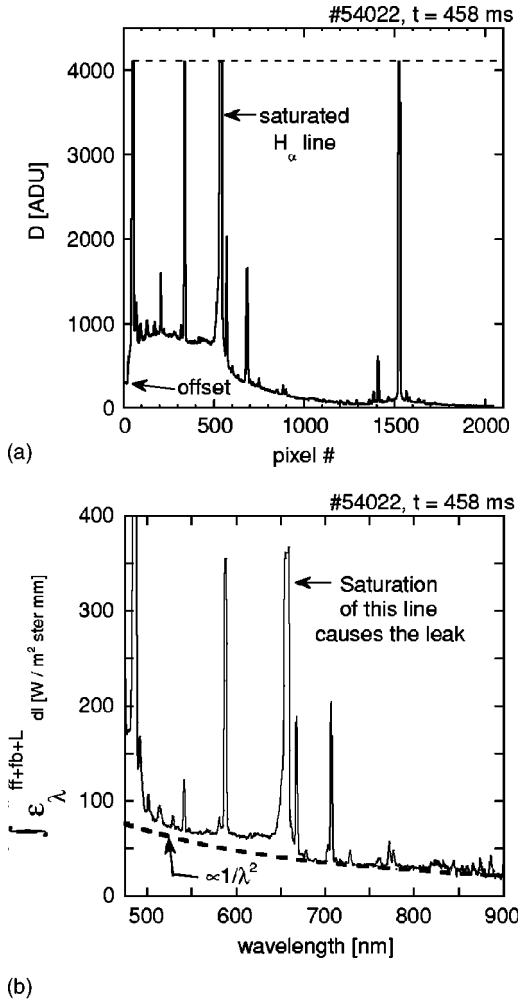

FIG. 6. (a) Measurement of plasma radiation in discharge No. 54022, $t = 458$ ms with several saturated lines. The offset value is higher by ≈ 180 ADUs than at an earlier time point which points to spurious signals. (b) The signal to the left of the H_α line is disturbed. This is obvious because this region does not fit to the $1/\lambda^2$ curve.

A different case is shown in Fig. 6. From plot (a) one can infer that the offset is enhanced by ≈ 180 ADUs. Here, according to point 2, a spurious signal is expected in the whole region on the lhs of the line. Indeed, Fig. 6(b) shows an inconsistency between the bremsstrahlung level on the lhs and on the rhs of the H_α line. This is clearly attributed to leakage.

VI. BAYESIAN MIXTURE MODELING

We apply Bayesian probability theory (BPT) to estimate Z_{eff} from noisy bremsstrahlung data, which is in addition superimposed with line emission radiation. BPT allows for the consistent combination of all information necessary to draw physical quantities from noisy data. In addition, BPT provides a tool for considering systematic effects that spoil the data. Such effects are given by systematic (calibration) uncertainties or data contributions which corrupt the physical effect to be studied. In the present case the physical effect of interest is the bremsstrahlung emission and the corrupting effect is given by superimposing line intensities. The nuisance line-emission contribution is considered properly in a physical model that describes the experimental data including both the bremsstrahlung intensity and the line intensities. The nuisance parameters of line-intensity amplitudes are marginalized in the framework of probability theory.

From the two basic rules of probability theory the sum and the product rule one can easily derive two rules being important for the statistical analysis described here.[8] Bayes theorem accounts for the combination of information in a probabilistic description,

$$p(X|Y,I) = \frac{p(Y|X,I)p(X|I)}{p(Y|I)}, \tag{7}$$

where X, Y denote events and I accounts for additional information to be specified for a comprehensive description of the inference problem. The marginalization rule

$$p(X|I) = \int_{-\infty}^{+\infty} p(X,Z|I)dZ = \int_{-\infty}^{+\infty} p(X|Z,I)p(Z|I)dZ \tag{8}$$

allows one to marginalize nuisance parameters by integration with respect to the prior distribution $p(Z|I)$. In addition, the marginalization rule provides a tool for consideration of systematic effects. Additional (nuisance) parameters are intro-

duced to model the systematic effects and are subsequently marginalized with respect to a prior distribution, that describes the (lack of) knowledge of the systematic parameters.

Starting from Bayes theorem, the probability density function (pdf) for Z_{eff} derived from the spectrometer data is obtained from

$$p(Z_{\mathrm{eff}}|D) = p(D|Z_{\mathrm{eff}})\frac{p(Z_{\mathrm{eff}})}{p(D)}, \tag{9}$$

where D denotes the measured data. Z_{eff} can be estimated from the posterior pdf $p(Z_{\mathrm{eff}}|D)$, which is the final result of the analysis. The posterior pdf can be decomposed according to Bayes theorem into the likelihood pdf $p(D|Z_{\mathrm{eff}})$, describing the probability of measuring data D, the prior pdf $p(Z_{\mathrm{eff}})$, accounting for all we know about Z_{eff} independent of the data, and a normalizing pdf $p(D)$.

The likelihood is obtained starting from a single pixel number i. A mixture model is employed to take into account the two alternatives that the pixel signal may be without or with line-radiation contributions, B_i and $\overline{B_i}$, respectively.[4,9] Different likelihood pdfs, $p(D_i|B_i,Z_{\mathrm{eff}})$ and $p(D_i|\overline{B_i},Z_{\mathrm{eff}})$ describe the two alternatives. The total likelihood for D_i is obtained by summing (marginalizing) over the two hypotheses B_i and $\overline{B_i}$

$$\begin{aligned} p(D_i|Z_{\mathrm{eff}}) &= p(D_i,B_i|Z_{\mathrm{eff}}) + p(D_i,\overline{B_i}|Z_{\mathrm{eff}}) \\ &= p(D_i|B_i,Z_{\mathrm{eff}})p(B_i|Z_{\mathrm{eff}}) \\ &\quad + p(D_i|\overline{B_i},Z_{\mathrm{eff}})p(\overline{B_i}|Z_{\mathrm{eff}}). \end{aligned} \tag{10}$$

The likelihood for the case where the measured intensity D_i exclusively consists of the bremsstrahlung intensity (hypothesis B_i) is given by a Gaussian distribution

$$p(D_i|B_i,Z_{\mathrm{eff}}) = \frac{1}{\sqrt{2\pi}\sigma_i}\exp\left(-\frac{[D_i - b_i(Z_{\mathrm{eff}})]^2}{2\sigma_i^2}\right), \tag{11}$$

assuming that the noise of the data D_i is normally distributed with variance σ_i^2. Here, $b_i(Z_{\mathrm{eff}})$ denotes the model function for the total signal including offset. Using the bremsstrahlung model, Eq. (3), the spectral transmission coefficient of the observation window glass T_i and the spectral sensitivity of the system E_i yields the model function

$$\begin{aligned} b_i(Z_{\mathrm{eff}}) &= O + \frac{T_i}{E_i}t_{\mathrm{exp}}\int_{\text{line of sight}}\varepsilon_i^{ff}(l)dl \\ &= O + \frac{T_i}{E_i}t_{\mathrm{exp}}\int_{\text{line of sight}}\frac{2.045\times10^{-29}n_e^2(l)}{\lambda_i^2 T_e^{0.35}(l)} \\ &\quad\times\exp\left(-\frac{12\,400}{\lambda_i T_e(l)}\right)Z_{\mathrm{eff}}dl, \end{aligned} \tag{12}$$

where t_{exp} is the exposure time.

The variance σ_i^2 consists of the variance from Eqs. (5) and (6) for the two spectrometer channels, respectively. Additional uncertainties, such as statistical errors of measurements on T_i and E_i, can be considered by adding a corresponding term including its variances to σ_i^2.[2,10] In the present data the statistical uncertainties of T_i and E_i are negligibly small compared with σ_i^2. Note that additional uncertainties may only be added to σ_i^2 if the errors are uncorrelated. Correlated errors occur, e.g., when T_i or E_i are uncertain with respect to an overall amplitude. This systematic uncertainty is addressed at the end of this section. The errors of the temperature and electron density profiles (measured with the Thomson scattering system) were not taken into account here but can be included analogically.

The corresponding likelihood for situation $\overline{B_i}$, where the measured signal contains in addition to bremsstrahlung intensity also line radiation S_i is

$$p(D_i|S_i,\overline{B_i},Z_{\mathrm{eff}}) = \frac{1}{\sqrt{2\pi}\sigma_i}\exp\left(-\frac{(D_i - b_i(Z_{\mathrm{eff}}) - S_i)^2}{2\sigma_i^2}\right). \tag{13}$$

The parameter S_i is necessary for describing data with line intensities. However, the value of S_i is unknown. Nuisance parameters such as S_i are marginalized

$$\begin{aligned} p(D_i|\overline{B_i},Z_{\mathrm{eff}}) &= \int_0^\infty p(D_i,S_i|\overline{B_i},Z_{\mathrm{eff}})dS_i \\ &= \int_0^\infty p(D_i|S_i,\overline{B_i},Z_{\mathrm{eff}})p(S_i)dS_i. \end{aligned} \tag{14}$$

The prior pdf $p(S_i)$ is chosen to be

$$p(S_i) = \frac{1}{\gamma}\exp\left(-\frac{S_i}{\gamma}\right), \quad \gamma = 1000, \tag{15}$$

which is the most uninformative pdf according to the maximum entropy principle with the constraint that the mean value is γ[11] $\cdot\gamma$ is chosen to be a typical amplitude for lines restricted by the constraint not to saturate the detector. Integration over S_i yields[4]

$$\begin{aligned} p(D_i|\overline{B_i},Z_{\mathrm{eff}}) &= \frac{1}{2\gamma}\left[1 + \mathrm{erf}\left(\frac{\gamma[D_i - b_i(Z_{\mathrm{eff}})] - \sigma_i^2}{\gamma\sqrt{2\sigma_i^2}}\right)\right] \\ &\quad\times\exp\left(\frac{-\gamma[D_i - b_i(Z_{\mathrm{eff}})] + (1/2)\sigma_i^2}{\gamma^2}\right) \end{aligned} \tag{16}$$

with the error function

$$\mathrm{erf}(x) = \frac{2}{\sqrt{\pi}}\int_0^x \exp(-z^2)dz. \tag{17}$$

This completes the two likelihood pdfs for the hypotheses B_i and $\overline{B_i}$. For obtaining the total likelihood in Eq. (10), the prior probabilities for the two hypotheses have to be specified. If we do not want to prefer *a priori* a hypothesis, we have to choose

$$p(B_i|Z_{\mathrm{eff}}) = p(\overline{B_i}|Z_{\mathrm{eff}}) = \tfrac{1}{2}. \tag{18}$$

Now, as the likelihood for a single data point $p(D_i|Z_{\mathrm{eff}})$ is given, the likelihood $p(D|Z_{\mathrm{eff}})$ of the measurement of the entire spectrum D (i.e., all exposed pixels) is given by multiplying the probabilities of the independent data

$$p(D|Z_{\mathrm{eff}}) = \prod_{i=25}^{2048} p(D_i|Z_{\mathrm{eff}}). \tag{19}$$

Finally, for obtaining the posterior pdf for Z_{eff}, Eqn. (9), the prior $p(Z_{\mathrm{eff}})$ has to be specified. To be uninformative about Z_{eff} we have chosen $p(Z_{\mathrm{eff}} \geqslant 1)$ to be constant and $p(Z_{\mathrm{eff}} < 1) = 0$. The data evidence $p(D)$, guaranteeing the posterior to be normalized, is independent of Z_{eff} and, therefore, not important for parameter estimation. Hence, $p(Z_{\mathrm{eff}}|D)$ is proportional to $p(D|Z_{\mathrm{eff}})$ for the interesting case of $Z_{\mathrm{eff}} \geqslant 1$.

In summary, the posterior pdf for Z_{eff} reads to be

$$p(Z_{\mathrm{eff}}|D) \propto p(D|Z_{\mathrm{eff}}) = \prod_{i=25}^{2048} \frac{1}{2}[p(D_i|B_i, Z_{\mathrm{eff}}) + p(D_i|\overline{B_i}, Z_{\mathrm{eff}})] \tag{20}$$

with Eqs. (11) and (16) for the likelihood pdfs.

The robust estimation of the bremsstrahlung background in the presence of nuisance line emission is due to the different shapes of the two likelihood distributions. The marginal likelihood, Eq. (16), decreases on a logarithmic scale for large D_i linearly with the difference $D_i - b_i$ on scale γ. In contrast, the exponent of the classical Gaussian likelihood, Eq. (11), decreases quadratically with $D_i - b_i$ on scale σ_i^2. The long tail of the marginal likelihood allows for a moderate fit of the data points with line emission in addition to the bremsstrahlung intensity b_i. The data points with bremsstrahlung intensity only are well described by the Gaussian likelihood, Eq. (11). The weight of the Gaussian likelihood is given by the normalizing constant which is much larger than that of the marginal likelihood. The reason is the smaller width of the Gaussian likelihood in comparison with that of the marginal likelihood. The outlier points, i.e., points with nuisance line emission, effectively have smaller weights in fitting the background. Consequently, the estimated bremsstrahlung intensity b_i is as close as possible to as many as possible data points whereas the data points which do not fit to b_i are down weighted according to the marginal likelihood.

An estimate for Z_{eff} is given by the maximum of the posterior pdf

$$\tilde{Z}_{\mathrm{eff}} = \max_{Z_{\mathrm{eff}}}\{p(Z_{\mathrm{eff}}|D)\}. \tag{21}$$

In order to estimate the uncertainty of $\tilde{Z}_{\mathrm{eff}}$, the Laplace approximation is applied. The second-order expansion on the posterior pdf $p(Z_{\mathrm{eff}}|D)$ at its maximum results in a Gaussian distribution with a standard deviation accounting for the estimation uncertainty of $\tilde{Z}_{\mathrm{eff}}$

$$\sigma_{\tilde{Z}_{\mathrm{eff}}} = \left(\left. \frac{d^2[-\ln p(Z_{\mathrm{eff}}|D)]}{(dZ_{\mathrm{eff}})^2} \right|_{Z_{\mathrm{eff}}=\tilde{Z}_{\mathrm{eff}}} \right)^{-1/2}. \tag{22}$$

The statistical measurement errors of the window-transmission spectral curve ΔT_i and the absolute-calibration spectral curve ΔE_i have to be considered equivalently to the statistical error of the bremsstrahlung spectrum. However, the systematic relative uncertainties $\Delta T_{\mathrm{sys}} = 0.01T$ and $\Delta E_{\mathrm{sys}} = 0.054E$ have to be considered differently, since they result in a correlated uncertainty for the complete bremsstrahlung spectrum. ΔE_{sys} comprises uncertainties of the calibration-lamp emissivity (2%) and uncertainties of transmission of the glass fibers (5%). The total systematic correlated uncertainty of 5.5% is large compared to the statistical uncertainty $\sigma_{\tilde{Z}_{\mathrm{eff}}}$ of Eq. (22). Since the model function $b_i(Z_{\mathrm{eff}})$ depends linearly on T and E, Eq. (12), the systematic uncertainty results in an additional relative uncertainty of $\tilde{Z}_{\mathrm{eff}}$ of $\approx 5.5\%$.

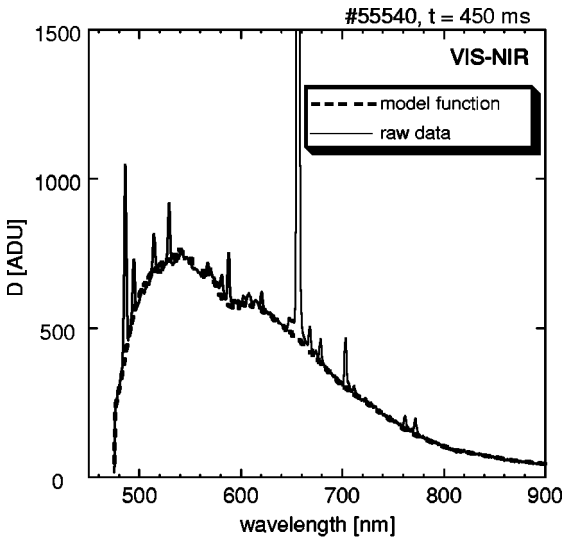

FIG. 7. Raw plasma light signal measured with the VIS-NIR channel at W7-AS. The dashed line shows the estimated background signal derived by means of Bayesian probability theory.

The formulas have been finally expanded for simultaneous estimation of Z_{eff} and the offset O, which can be derived from the first 24 pixels of the detector not exposed to plasma light. However, dark exposure measurements have shown that the offset in the exposed pixels can differ from the offset provided by the 24 covered pixels. This could easily cause an estimation change of Z_{eff} by up to 10% at discharges with low signals. In order to estimate the offset jointly with Z_{eff}, O in model function, Eq. (12), is treated as a variable, instead of setting it to the offset value derived from the 24 covered pixels of the detector. The unreliable information provided by the 24 covered pixels is not used. The data from these pixels are not necessary to estimate O since the wavelength dependence of the model function clearly separates from the offset O. Estimates for both Z_{eff} and O are provided by maximizing the posterior pdf with respect to both variables.

The entire algorithm has been implemented in a C code which returns $\tilde{Z}_{\mathrm{eff}}$ and $\tilde{O}$ and their respective errors. For a time instant of interest of a plasma discharge the analysis requires ≈ 1 s CPU time on a 1 GHz PC.

VII. RESULTS

Figure 7 shows an example of a raw plasma emission signal measured with the VIS-NIR channel (solid line). The data are from plasma discharge No. 55540 at discharge time $t = 0.45$ s. The dashed line represents the fit of the background signal as obtained by Bayesian modeling, described

in Sec. VI. The estimated background closely fits the data points excluding line emission. Pixels with line emission are implicitly treated as outliers.

The robust technique presented in this paper results in a reliable background estimates if there are enough pixels with exclusively background intensity and if the data uncertainties are reliable. Data uncertainties that are estimated to be too large result in overestimation of Z_{eff} because pixels with line emission are taken as regular data points. On the other hand, data uncertainties that are estimated to be too small yield an underestimated Z_{eff} value since excessive regular data points with exclusively bremsstrahlung intensity are treated as line emission outliers. This makes careful estimation of data uncertainties being of importance.

Each data point can be classified with a probability of containing only bremsstrahlung intensity or if there is additional line emission. The probability for hypothesis B_i of having only bremsstrahlung intensity is approximately[9]

$$p(B_i|D_i) \approx p(B_i|D_i,\tilde{Z}_{\mathrm{eff}}) = \frac{p(B_i)p(D_i|B_i,\tilde{Z}_{\mathrm{eff}})}{p(B_i)p(D_i|B_i,\tilde{Z}_{\mathrm{eff}}) + p(\overline{B_i})p(D_i|\overline{B_i},\tilde{Z}_{\mathrm{eff}})}. \quad (23)$$

In principle, the quantity of interest is $p(B_i|D_i)$ where Z_{eff} is marginalized. However, for well determined estimates of $\tilde{Z}_{\mathrm{eff}}$ the integral can be approximated by the integrand at the maximum value $\tilde{Z}_{\mathrm{eff}}$. Figure 8(a) shows classified data points. Gray points depict data with background probability greater than 50% and black points with less than 50%. Most of the data points contain no line-radiation contribution which makes the bremsstrahlung estimate robust. The averaged background probability $N^{-1}\Sigma_{i=1}^{N} p(B_i|D_i,\tilde{Z}_{\mathrm{eff}})$ is 0.79. This means that ≈80% of the data points contain bremsstrahlung intensity only.

The robust fit of the spectrum to a bremsstrahlung model is most clearly shown with the residuum $(D_i - b_i)/\sigma_i$. For a reasonable fit, the data points with only bremsstrahlung intensity have to be within a few standard deviations around the estimated b_i. Data points with additional line emission do not have to fulfill this criterion since they are treated as outliers. Figure 8(b) shows the residuum for the same spectrum as in Fig. 8(a). The amplitude of the oscillations due to random uncertainties lies in the range of a few σ_i, which confirms the validity of the uncertainty assessment. However, systematic deviations, in addition to emission lines, deteriorate the residuum. The systematic structures can be mainly found at small wavelengths and at the bump between 580 and 620 nm [see Fig. 8(a)]. The residual structures are interpreted as systematic errors in the absolute calibration of T and E, not considered appropriately. An elaborate study of these systematic effects is beyond the scope of this paper.

Finally, Fig. 9 shows a result of Z_{eff} with both spectrometer channels in a discharge with carbon pellet injection at $t=618$ ms. Z_{eff} increases rapidly to a value ~2 due to ionization of pellet material and subsequently drops due to radial transport of carbon ions removing them out of the plasma. The drop-off time shows already the time scale of the carbon confinement time of about 50 ms. The Z_{eff} value

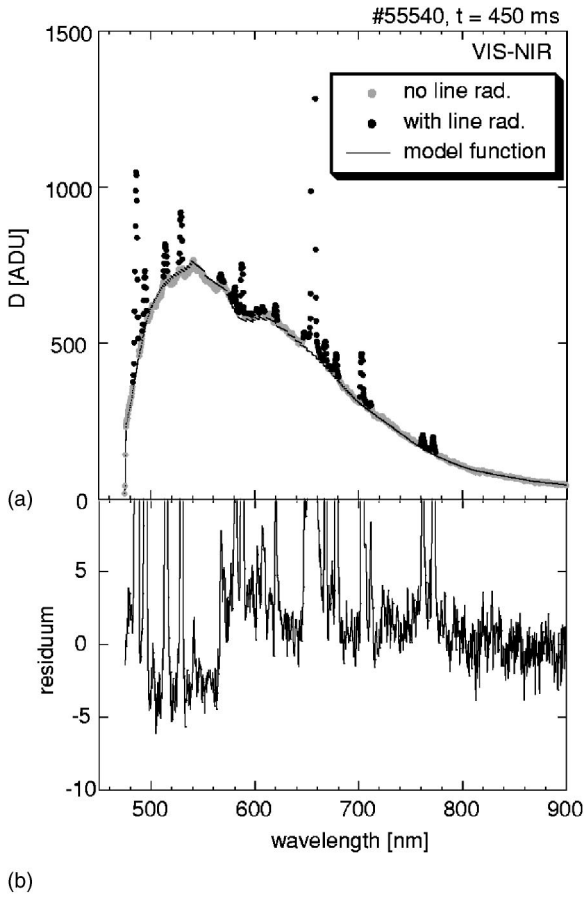

FIG. 8. (a) Data points classified with a cutoff background probability of 50%. Gray points denote data with probability of >50% of being pure bremsstrahlung whereas black points denote data with probability of >50% having line-radiation contribution. (b) Residuum for the background estimation.

for the time point shortly before the pellet injection already shows an increased Z_{eff} because of time averaging over 7 ms.

VIII. SUMMARY

The effective charge Z_{eff} of fusion plasmas was estimated from spectroscopic bremsstrahlung measurements em-

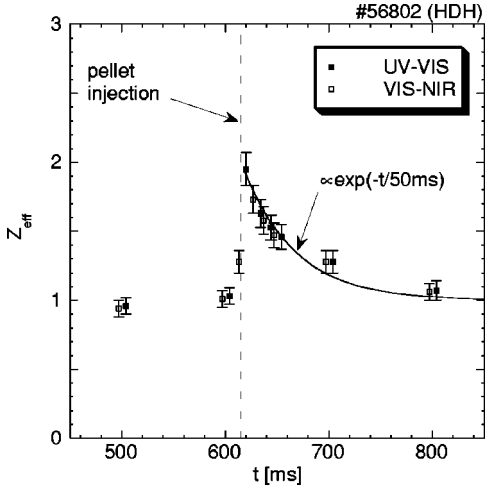

FIG. 9. Z_{eff} measurement with both spectrometer channels in a high density high confinement mode discharge with carbon pellet injection.

ploying Bayesian probability theory. A microspectrometer has been used to measure the spectral distribution of the bremsstrahlung intensity. The spectral resolution allows one to separate spectral regions with bremsstrahlung emission from regions where additional nuisance line emission occurs. A Bayesian mixture model provides a consistent tool to model the bremsstrahlung intensity in the presence of line intensity. The robust estimation of Z_{eff} treats pixels with nuisance line intensity as outliers which need not to be deleted from the data prior to the fitting procedure. Hence, the complete bremsstrahlung spectrum can be analyzed without censoring the data. Our robust technique results in reliable bremsstrahlung estimates if there are enough pixels with only bremsstrahlung intensity and if the data uncertainties are correctly estimated.

The applied spectrometer, consisting of two channels covering the wavelength region of 250–1100 nm, has been absolutely calibrated using an Ulbricht sphere. The reliable wavelength region is $400<\lambda<920$ nm. The saturation behavior and the linearity of the detectors were studied to determine the proper conditions of the experimental setup. A comprehensive investigation of the statistical and systematic uncertainties of the spectroscopic and calibration data are vital for a reliable estimation of Z_{eff}.

The use of two adjacent toroidal lines of sight provided consistent estimates of the line-averaged Z_{eff} values. The redundancy of one of the two lines of sight allows to simplify the bremsstrahlung experimental setup for the future fusion experiment W7-X.

ACKNOWLEDGMENT

The authors would like to thank Mr. Andre John for technical assistance.

[1] A. T. Ramsey, Rev. Sci. Instrum. **58**, 1211 (1987).
[2] R. Fischer, C. Wendland, A. Dinklage, S. Gori, and V. Dose, Plasma Phys. Controlled Fusion **44**, 1501 (2002).
[3] R. W. T. König *et al.*, *Active Spectroscopy on JET and ITER*, in Diagnostics for Experimental Thermonuclear Fusion Reactors 2, edited by P. E. Stott *et al.*(Plenum, New York, 1998).
[4] R. Fischer, K. M. Hanson, V. Dose, and W. von der Linden, Phys. Rev. E **61**, 1152 (2000).
[5] I. H. Hutchinson, *Principles of Plasma Diagnostics* (Cambridge University Press, Cambridge, 2002).
[6] S. Morita and J. Baldzuhn, *Z_{eff} Measurement and Analysis of Reheat-Mode Discharges in W7-AS*, IPP III/199 (Max-Planck-Institut für Plasmaphysik, Garching, 1994).
[7] D. F. Grey, *The Observation and Analysis of Stellar Photospheres* (Cambridge University Press, Cambridge, 1992).
[8] D. S. Sivia, *Data Analysis. A Bayesian Tutorial* (Clarendon, Oxford, 1996).
[9] R. Fischer, K. M. Hanson, V. Dose, and W. von der Linden, *Bayesian Background Estimation*, in Bayesian Inference and Maximum Entropy Methods in Science and Engineering, edited by C. R. Smith, J. T. Rychert, and G. J. Erickson (AIP, Melville, NY, 2001), pp. 193–212.
[10] V. Dose, R. Fischer, and W. von der Linden, *Deconvolution Based on Experimentally Determined Apparatus Functions*, Bayesian Inference and Maximum Entropy Methods in Science and Engineering, edited by G. J. Erickson (Kluwer Academic, Dordrecht, 1998), pp. 147–152.
[11] L. R. Mead and N. Papanicolaou, J. Math. Phys. **25**, 2404 (1984).